Clays and Clay Minerals, Vol. 47, No. 4, 439–457, 1999.

THE STRUCTURE OF U^{6+} SORPTION COMPLEXES ON VERMICULITE AND HYDROBIOTITE

ERIC A. HUDSON,[1,†] LOUIS J. TERMINELLO,[1] BRIAN E. VIANI,[2] MELISSA DENECKE,[3] TOBIAS REICH,[3] PATRICK G. ALLEN,[1,4] JEROME J. BUCHER,[4] DAVID K. SHUH,[4] AND NORMAN M. EDELSTEIN[4]

[1] Glenn T. Seaborg Institute for Transactinium Science, Lawrence Livermore National Laboratory, L-231, P.O. Box 808, Livermore, California 94551, USA

[2] Earth and Environmental Sciences Directorate, Lawrence Livermore National Laboratory, L-219, P.O. Box 808, Livermore, California 94551, USA

[3] Institut für Radiochemie, Forschungszentrum Rossendorf, Postfach 510119, D-01314 Dresden, Germany

[4] Lawrence Berkeley National Laboratory, MS 70A-1150, 1 Cyclotron Rd., Berkeley, California 94720, USA

Abstract—The sorption of the uranyl oxo-cation (UO_2^{2+})at different types of binding sites on layer silicate mineral surfaces was investigated. Well-characterized samples of vermiculite and hydrobiotite were exposed to aqueous uranyl under conditions designed to promote surface sorption either at fixed charge ion-exchange sites or at amphoteric surface hydroxyl sites. The local structure of uranium in the sorption samples was directly measured using uranium L_3-edge extended X-ray absorption fine structure (EXAFS). Polarized L_1- and L_3-edge X-ray absorption near-edge structure (XANES) measurements were used to characterize the orientation of uranyl groups in layered samples. X-ray diffraction (XRD) measurements of interlayer spacings were used to assess the effects of ion-exchange and dehydration upon the mineral structure. The most significant findings are: (1) Under conditions which greatly favor ion-exchange sorption mechanisms, uranyl retains a symmetric local structure suggestive of an outer-sphere complex, with a preferred orientation of the uranyl axis parallel to the mineral layers; (2) Upon dehydration, the ion-exchange complexes adopt a less symmetric structure, consistent with an inner-sphere complex, with less pronounced orientation of the uranyl axis; and (3) For conditions which favor sorption at surface hydroxyl sites, uranyl has a highly distorted equatorial shell, indicative of stronger equatorial ligation, and the detection of a neighboring U atom suggests the formation of surface precipitates and/or oligomeric complexes.

Key Words—Cation Exchange, EXAFS, Sorption, Surface Complex, Uranium, Uranyl, Vermiculite, XANES, XRD.

INTRODUCTION

Transport of uranium in the geosphere is a complex phenomenon which is not yet fully characterized. Uranium migration is a concern both in the management of contaminated sites and in the planning of waste-disposal installations. There is a growing effort to improve the understanding of the processes which control U transport, both to facilitate remediation of contaminated sites and to improve the prediction of migration behavior. One such process is the retardation of U transport in ground water due to sorption on mineral surfaces. Despite the importance of this mechanism, there is limited direct knowledge about U-mineral interactions at the molecular level. Thus, we have investigated the structure of U bound at different binding sites on layer silicate surfaces.

In contact with air and water, U exists predominantly in the +6 oxidation state as the linear uranyl oxo-cation UO_2^{2+}. Our examination of U immobilization on mineral surfaces begins with a consideration of the aqueous chemistry of uranyl. Although the two axial oxygen atoms are tightly bonded to the U atom, there are four to six additional coordination sites available about the equator of the uranyl cation. In fact, uranyl exhibits a rich coordination chemistry through these equatorial sites, with strong complexation by hydroxide and carbonate among the many possibilities (Grenthe *et al.*, 1992). Uranyl may similarly be expected to form inner-sphere complexes at active sites on a mineral surface, with surface O atoms acting as equatorial ligands. Uranyl also tends to form oligomers in aqueous solution, especially at neutral or high pH, or in the presence of ligands which favor bridged structures (Grenthe *et al.*, 1992; Allen *et al.*, 1996a). Oligomeric surface complexes or surface precipitates are therefore strong possibilities in the interaction of uranyl with minerals. Aqueous uranyl also may coordinate to cation-exchange sites in many materials, such as clays and zeolites (Suib *et al.*, 1986). The selectivity of montmorillonite ion-exchange sites for uranyl is between those of divalent and monovalent metal cations (Tsunashima *et al.*, 1981). The following investigation of uranyl interaction with layer silicate surfaces considers several potential sorption mechanisms, including inner- and outer-sphere complexation, oligomeric surface complexation, ion-exchange complexation, and surface precipitation. These mechanisms are not

[†] Present address: Lam Research Corp., CA-3, 4650 Cushing Pkwy., Fremont, California 94538, USA.

Copyright © 1999, The Clay Minerals Society

https://doi.org/10.1346/CCMN.1999.0470406 Published online by Cambridge University Press

exclusive and in fact some combinations are possible. In this paper, any immobilization of uranyl on external or interlamellar layer silicate surfaces is generally referred to as "sorption".

Sorption sites for aqueous metal species on phyllosilicate minerals are placed in two categories based on the sorption mechanism and the local structure of the mineral surface: (1) Ion-exchange at permanent negative charge sites; and (2) Complexation by chemically active surface hydroxyl groups at layer edges. The experiments presented here show trends in uranyl local structure as conditions are varied to favor sorption at these two different types of sites. The possibility for such control arises from a combination of sorption properties. Complexation at surface hydroxyl sites becomes more likely as pH values increase, due to deprotonation of active groups (Sposito, 1984). This complexation can also be promoted by increasing the number of edge sites, *i.e.*, by using a smaller size fraction of the mineral. These conditions also promote precipitation of surface-stabilized solid phases on mineral faces with exposed surface hydroxyl sites. Ion exchange is favored at lower ionic strengths, where there is less competition from background cations. In these experiments, ion-exchange interactions are promoted by maintaining low pH and low ionic strength, and in some cases by pre-exchanging with an easily removable monovalent cation. Surface complexation and/or surface precipitation at hydroxyl sites are promoted by using near-neutral pH, increased mineral surface areas, and higher ionic strength. The aqueous speciation of uranyl is strongly pH dependent, so geochemical modeling based on thermodynamic data was used to predict the uranyl species, aiding in the interpretation of sorption trends. In fact, near-neutral pH tends to favor neutral or anionic uranyl species, reducing the likelihood of sorption by cation exchange.

This work also develops frontier techniques for the study of uranyl sorption. We directly measured the local structure of U in the sorption samples using X-ray absorption spectroscopy (XAS). This *in situ* probe of local atomic and electronic structure demonstrated considerable value to study surface sorption on minerals (Brown, 1990). XAS measurements are inherently element specific due to the characteristic binding energies of core electrons. The ability to obtain structural information only in the neighborhood of the element of interest allows the study of dilute species in a complex hydrated matrix. XAS is commonly divided into two overlapping techniques: X-ray absorption near-edge structure (XANES) and extended X-ray absorption fine structure (EXAFS). XANES focuses on spectral details at X-ray energies near the ionization threshold for a given core electron, providing information on site symmetry and oxidation state. By using X-ray energies 50–1500 eV above the ionization threshold, EXAFS extracts bonding information for the first few atomic shells around the target element, including coordination numbers and interatomic distances. EXAFS was previously used to probe the local structure of U bound to several different mineral surfaces (Dent *et al.*, 1992; Chisholm-Brause *et al.*, 1994; Waite *et al.*, 1994). Some of those results are discussed below.

The XAS studies described in this paper include the application of U EXAFS to powder samples, and specialized XANES measurements, which characterize the orientation of uranyl groups in layered structures. If mineral sorption samples can be created with a known macroscopic orientation of the crystal lattice, the polarization dependence of uranium L_1- and L_3-edge XANES spectra can be exploited to characterize the molecular orientation of entrained uranyl species. In the present experiments, layered mineral structures were exposed to uranyl under conditions which favor extensive interlamellar ion-exchange. By comparing XANES spectra measured with the x-ray plane polarization vector either parallel or perpendicular to the structural layers, we have characterized the orientation of the uranyl cation with respect to the structural layers. To our knowledge, this is the first application of polarization-dependent XANES to the study of uranyl sorption. In fact, one purpose of the present work is to introduce polarization-dependent XANES as a unique probe of uranyl orientation in mineral samples. Another goal of this study is to better establish EXAFS as a probe of uranyl sorption chemistry.

Expandable phyllosilicate minerals were selected for sorption experiments. Vermiculite and a regularly interstratified biotite-vermiculite, hydrobiotite, were used both with and without modification. These minerals are available in large homogeneous crystals, allowing the production of powders with specific size fractions and with uniform composition. Furthermore, slices from these crystals provided oriented samples for the polarization-dependent XANES measurements. Structural changes in these minerals are easily followed by X-ray diffraction (XRD) measurements of the basal-plane interlayer spacing, $d(001)$.

Apart from its immediate significance in the area of U migration, the present work is also relevant to other environmentally hazardous actinides, such as neptunium, plutonium, and americium. The uranyl cation provides a direct analog for other actinyl species, *e.g.*, PuO_2^{2+} and PuO_2^{+}, but with a significantly simplified redox chemistry. Furthermore, the XAS tools developed here for uranyl are applicable to other actinyl species. From a practical standpoint, the natural isotopes of U are much easier to handle than the available isotopes of these other actinides, which are highly radioactive. This provides additional motivation to develop a detailed understanding of U sorption as a basis for much more challenging experiments on other actinides.

https://doi.org/10.1346/CCMN.1999.0470406 Published online by Cambridge University Press

MATERIALS AND METHODS

Mineral preparation

Vermiculite (Sanford, North Carolina) was obtained from Ward's Natural Science Establishment, Rochester, New York, USA, and hydrobiotite (labeled as "vermiculite", Palabora open pit, Phalaborwa, Transvaal, Republic of South Africa) was obtained from Mineralogical Research Co., San Jose, California, USA. The sorption experiments used two different size fractions of the ground minerals, as well as slices cut from the best parts of the samples. Portions of each mineral were ground in an alumina shatterbox, in contact with deionized water. Fractions with particle sizes <45 μm and from 45 to 250 μm were separated by wet sieving. Thin slices, ~1.2 × 0.8 × 0.1 cm, were cut and lightly polished from epoxy-mounted crystals of each mineral. The large faces are perpendicular to the (001) cleavage plane. This provided a sufficiently large sample with a well-defined orientation for use in the angle-dependent XAS experiments.

To adjust the accessibility of interlayer-cation exchange sites, portions of each mineral were treated to replace the exchangeable cations. Starting with the 45–250 μm size fractions, Li^+-exchanged vermiculite and hydrobiotite samples were prepared by three successive treatments with 1.0 M LiCl at 60°C. The slices were also Li^+-exchanged using a similar process at room temperature. The <45 μm size fractions were used to prepare K^+-exchanged vermiculite and hydrobiotite. The minerals were treated twice with 0.1 M KCl, once at 65°C and again at room temperature, and then baked at 220°C for 5 h. Dried samples of the unmodified minerals were also prepared, using the 45–250 μm size fractions, by storing for one day in a vacuum desiccator at room temperature. These samples were maintained under argon gas and double-sealed in 0.10 mm polyethylene (PE) bags, along with anhydrous $CaSO_4$ desiccant in each bag.

Mineral characterization

Specific surface areas of the minerals, after grinding, were measured by BET analysis, using nitrogen gas adsorption in a Micromeritics Instrument Corp. system, model ASAP 2000. The qualitative elemental compositions of the minerals were determined from X-ray fluorescence spectra. Spectra were measured using a Hitachi Model S-800 Scanning Electron Microscope with a 25 kV beam energy and a Kevex 8000 Energy Dispersive Spectroscopy (EDS) system with a Quantum window.

The cation exchange capacity (CEC) was measured by initially loading the mineral exchange sites with Na^+, and then removing the Na^+ by exchanging with Mg^{2+}. Half-gram portions of finely ground mineral (<45 μm) were treated with a 1.0 M NaCl solution, rinsed with a 0.010 M NaCl solution, and then treated with a 0.50 M $MgCl_2$ solution. Each treatment comprised shaking the mineral with three successive 45-mL aliquots of the solution for >2 h. The $MgCl_2$ solutions were combined and analyzed to determine the amount of Na^+ released. The concentration of Na^+ was measured by inductively coupled plasma atomic emission spectroscopy (ICP-AES), using a Fisons Instruments/Applied Research Laboratories Model 3560B ICP Analyzer with an Optical Emission Spectroscopy Direct Reader. Duplicate analyses for each mineral gave results which agreed within the expected uncertainty ranges.

Preparation of uranium-mineral samples

Uranium-mineral sorption samples were prepared by exposing the minerals to aqueous solutions of uranyl. All chemicals used were reagent grade. A Milli-Q Reagent Water System from Millipore Corp. provided deionized (DI) water with a resistivity >14 MΩ cm. Samples were prepared in air at room temperature and no special measures were taken to exclude carbon dioxide. Solution pH values were measured using an Orion 8103 Ross combination electrode and an Orion Research 601A Digital Ionanalyzer pH meter.

Details about each U sorption sample are given in Table 1. The mineral mass was 100 mg for each sample, except for the ~200 mg oriented slices, V-OR and HB-OR. The -IE2, -IE3, -SC, and -SCK samples were prepared as follows. The volume of the exposure solution was 0.500 L. After 4 d stirring in high density PE bottles, the solid phase was separated by filtration, rinsed with 200 mL DI water, and packaged for XAS analysis without drying. Uptake of U by the mineral was determined by measuring the U concentration in solution before and after treatment. Uranium concentrations were determined by ICP-AES and/or by ICP-mass spectroscopy using a Fisons Instruments Model PQ1 ICP-MS.

Samples V-IE1, HB-IE1, V-OR, and HB-OR, were treated differently. For the -IE1 samples, the exposure volume was 40 mL, whereas the -OR pair used 15 mL. To maximize the loading of uranyl onto ion-exchange sites, these four samples were exposed to three successive aliquots of their stock solutions. A large mass action effect is achieved through the combination of relatively high uranyl concentrations and multiple exposures. In addition, the Li^+-exchanged minerals were used for these samples because the monovalent Li^+ is more easily displaced than the natural divalent Mg^{2+} interlayer cation. These treatments were performed in polypropylene centrifuge cones. The minerals were shaken 1–4 d with each aliquot and the solid phase was separated by filtration, centrifugation and/or decanting. Samples were rinsed twice with 40 mL of DI water and packaged for XAS analysis without drying.

After initial XAS analysis, samples V-IE1, HB-IE1, and V-OR were aged 3 mo and then dried overnight

https://doi.org/10.1346/CCMN.1999.0470406 Published online by Cambridge University Press

Table 1. Summary of U sorption samples.

Sample[1]	Mineral (size fraction)	Initial $[UO_2^{2+}]$ (counter-ion)	Initial pH	Final pH	Additional electrolyte	Uptake of U	Description
V-IE1[2]	Li^+-exchanged vermiculite (45–250 μm)	1.7×10^{-2} M (NO_3^-)	2.6	—	—	—	Uranyl ion exchange, large mass action, monovalent cation
HB-IE1[3]	Li^+-exchanged hydrobiotite (45–250 μm)	1.7×10^{-2} M (NO_3^-)	2.6	—	—	—	Uranyl ion exchange, large mass action, monovalent cation
V-IE2	Vermiculite (45–250 μm)	9.2×10^{-4} M (NO_3^-)	2.0	1.8	—	9.5%	Uranyl ion exchange
HB-IE2	Hydrobiotite (45–250 μm)	9.2×10^{-4} M (NO_3^-)	2.0	1.8	—	11.4%	Uranyl ion exchange
V-IE3	Vermiculite (<45 μm)	1.1×10^{-4} M (Cl^-)	2.4	2.5	—	3.6%	Uranyl ion exchange, low loading
HB-IE3	Hydrobiotite (<45 μm)	1.1×10^{-4}M (Cl^-)	2.5	2.6	—	2.7%	Uranyl ion exchange, low loading
V-SC	Vermiculite (<45 μm)	3.2×10^{-6} M (Cl^-)	6.5	6.9	5.0×10^{-4} M $MgCl_2$	77.6%	Promote surface complexation
HB-SC	Hydrobiotite (<45 μm)	3.2×10^{-6} M (Cl^-)	6.5	7.1	5.0×10^{-4} M $MgCl_2$	53.9%	Promote surface complexation
V-SCK	K^+-exchanged vermiculite (<45 μm)	2.8×10^{-6} M (Cl^-)	6.5	7.5	1.0×10^{-3} M KCl	33.0%	Promote surface complexation, partly collapsed interlayer
HB-SCK	K^+-exchanged hydrobiotite (<45 μm)	2.8×10^{-6} M (Cl^-)	6.5	7.7	1.0×10^{-3} M KCl	62.8%	Promote surface complexation, collapsed interlayer
V-OR[4]	Li^+-exchanged vermiculite (oriented slice)	1.7×10^{-2} M (NO_3^-)	2.6	—	—	—	Uranyl ion exchange, large mass action, monovalent cation
HB-OR	Li^+-exchanged hydrobiotite (oriented slice)	1.7×10^{-2} M (NO_3^-)	2.6	—	—	—	Uranyl ion exchange, large mass action, monovalent cation

[1] V- refers to vermiculite, HB- refers to hydrobiotite; -IE refers to ion-exchange samples, -SC refers to surface complexation samples.
[2] Dehydrated sample is V-IE1-D.
[3] Dehydrated sample is HB-IE1-D.
[4] Dehydrated sample is V-OR-D.

in a vacuum desiccator at room temperature and repackaged under argon gas. These dry samples, referred to here as V-IE1-D, HB-IE1-D, and V-OR-D, respectively, were again analyzed by XAS.

X-ray diffraction

XRD patterns were measured using a Cu-anode Scintag PAD-V powder X-ray diffraction system with a Kevex Psi Peltier-cooled SiLi X-ray detector, gated to accept only CuKα radiation. Because the *d*(001) value was important, most samples were spread onto a stainless steel plate to enhance the horizontal orientation of platelets and thus the (00*l*) reflections. Dried samples were examined in double-sealed PE bags.

Prediction of uranium speciation

The speciation of the uranyl ion in solution may influence the sorption mechanism. This speciation is predicted from known, and mostly controllable, experimental parameters, by using the EQ3NR geochemical modeling program with the GEMBOCHS thermodynamic database (version R16), both developed at Lawrence Livermore National Laboratory. These thermodynamic parameters are based, in part, upon a critical compilation of U constants by Grenthe *et al.* (1992). The formation constant K_f for the neutral hydrolysis product $UO_2(OH)_2$ (aq) is one of several important in predicting U speciation at near-neutral pH. However Grenthe *et al.* recommended only a limiting value, log $K_f < -10.3$, for this species. Therefore the predictions are based on two sets of calculations—one assuming this limiting value for log K_f (as in the GEMBOCHS database) and another using the value log $K_f = -12$, given by Lemire and Tremaine (1980).

Table 2 shows U speciation predictions for selected conditions, representative of the solutions used here for sample preparation. Calculations used parameters for 25°C, for comparison to experiments performed at room temperature (~20°C). Carbonate and bicarbonate concentrations were determined by assuming equilibrium with air. The background electrolyte (KCl or

https://doi.org/10.1346/CCMN.1999.0470406 Published online by Cambridge University Press

Table 2. Dependence of calculated uranyl speciation upon total U concentration, pH, and formation constant K_f.

Uranyl species	Percentage[1] of total UO_2^{2+}		
	$[U]_T = 1.7 \times 10^{-2}$ M pH = 2.6	$[U]_T = 3.0 \times 10^{-6}$ M pH = 6.5 log $K_f = -10.3$[2]	$[U]_T = 3.0 \times 10^{-6}$ M pH = 6.5 log $K_f = -12$[3]
UO_2^{2+}	94.0	—	—
$UO_2(OH)_2(aq)$	—	78.3	3.6
$(UO_2)_2CO_3(OH)_3^-$	—	15.0	72.8
UO_2OH^+	—	3.3	7.3
$UO_2CO_3(aq)$	—	1.7	3.7
$(UO_2)_3(OH)_5^+$	—	1.0	10.4
$UO_2NO_3^+$	2.8	—	—
$(UO_2)_2OH^{3+}$	2.6	—	—

[1] Values <1% are not listed.

[2] Assumed value for the $UO_2(OH)_2(aq)$ formation constant (from Grenthe *et al.*, 1992). See text for details.

[3] Alternative assumed value for the $UO_2(OH)_2(aq)$ formation constant (from Lemire and Tremaine, 1980). See text for details.

$MgCl_2$) had little influence on U speciation. For samples prepared with pH < 3, the predominant U species in the starting solutions was the free uranyl aquo cation UO_2^{2+}. For these low-pH systems, the aquo cation accounted for >98% of the U, except for the 0.017 M uranyl nitrate solutions, as shown in Table 2. For solutions prepared with pH = 6.5, the predicted composition includes several major U species and is influenced greatly by the choice of K_f. If the limiting value of Grenthe *et al.* (1992) for K_f is used, the predominant species is $UO_2(OH)_2$ (aq). However the value of K_f from Lemire and Tremaine (1980) leads to a distribution where $UO_2(OH)_2$ (aq) is a minor component and $(UO_2)_2CO_3(OH)_3^-$ is predominant. Representative plots of U speciation *vs.* pH were presented for the former (Prikryl *et al.*, 1994) and the latter (Waite *et al.*, 1994). In either case, uranyl is mainly in neutral or anionic forms at pH = 6.5 and the extent of cation exchange interactions with a substrate is thereby reduced.

Any study of uranyl-sorption chemistry at near-neutral pH must consider the possibility of precipitating hydrous uranyl hydroxides, such as schoepite, $UO_2(OH)_2 \cdot H_2O$. The strong hydrolysis properties of the uranyl ion can lead to the formation of these fairly insoluble solids even at U concentrations $<10^{-5}$ M. Ideally, exposure conditions are designed to maintain concentrations below saturation levels with respect to these solid phases, thereby insuring that any observed U deposition represents a genuine chemical interaction with the mineral rather than simple precipitation of a bulk phase. This requirement presents challenges in the preparation of sorption samples for detailed EXAFS analysis, which requires moderate concentrations of U (>0.1 wt. %). To obtain such solid samples at near-neutral pH values, we used U solution concentrations close to saturation values. Calculations predict a solution which is unsaturated for all known solids, using the initial conditions selected for the exposures, if the limiting value for K_f from Grenthe *et al.* (1992) is assumed. If the value from Lemire and Tremaine (1980) is used, the initial solutions are slightly beyond the saturation limit for schoepite. However, simulations based upon the measured *final* U concentrations and pH values indicate sub-saturation conditions for these exposures, for either choice of K_f. Therefore schoepite precipitation cannot be the sole sorption mechanism for any of the samples prepared at near-neutral pH.

Another solid phase of concern is soddyite, $(UO_2)_2SiO_4 \cdot 2H_2O$, which has a known solubility constant (Nguyen *et al.*, 1992). After exposure, some of the near-neutral pH solutions were beyond saturation concentrations for this solid. This situation is difficult to avoid, because even trace dissolution of the mineral substrate can introduce sufficient silicic acid into solution to exceed the solubility limit of soddyite at near-neutral pH. The final Si concentration, measured by ICP-AES, was $3–4 \times 10^{-6}$ M for the near-neutral V-SC, HB-SC, V-SCK, and HB-SCK samples. These conditions allow the precipitation of soddyite.

X-ray absorption spectroscopy

Measurement. The uranium L_3-edge X-ray absorption spectra presented here were measured on several beamlines. Beamline X23A2 at the National Synchrotron Light Source (NSLS) is a bend-magnet line equipped with a Si(311) double-crystal monochromator (DCM). Beamline II-3 at the Stanford Synchrotron Radiation Laboratory (SSRL) is a bend-magnet line with a Si(220) DCM. Beamlines IV-1 and IV-3 at SSRL are similar wiggler lines with Si(220) DCMs. Spectra were collected in transmission mode using Ar ionization chambers to measure the incident and transmitted X-ray flux. Additional spectra were collected on beamlines II-3 and IV-1 using a solid-state Ge X-ray detector (Bucher *et al.*, 1996) to selectively monitor the uranium L_α X-ray fluorescence line. This fluorescence signal is proportional to the absorption of X-rays associated with the uranium L_3 edge. For every scan, the monochromator energy was calibrated by simultaneous measurement of the transmission spectrum of a solid uranyl nitrate hexahydrate standard, placed in the X-ray beam downstream from the sample. The white-line maximum in the spectrum of the standard was assumed to be at 17,175 eV, to agree with published values (Petiau *et al.*, 1986). To avoid undesirable higher-energy X-rays arising from the diffraction harmonics, the SSRL monochromators were detuned to 50% of maximum flux. The NSLS beam contained very little harmonic content and a feedback system continuously adjusted the monochromator to maintain maximum flux. For the polarized XANES studies, ad-

https://doi.org/10.1346/CCMN.1999.0470406 Published online by Cambridge University Press

ditional spectra were collected in transmission mode at the uranium L_1 edge.

Powder samples were mounted in 1.5-mm thick PE holders with 17 × 2 mm slots, and held in place with 0.08 mm Mylar tape. The holders were oriented at 45° to the incident beam, allowing the simultaneous measurement of fluorescence and transmission spectra. For these samples, the beam size was typically 9 × 1 mm. For polarization-dependent measurements, the thin mineral slices were mounted normal to the beam. For these samples, spectra were collected in transmission mode with a beam size of typically 3 × 0.5 mm. All samples were double-sealed in 0.05 mm PE bags for safety purposes. Dried samples were double-sealed in 0.10-mm PE bags and packaged with anhydrous $CaSO_4$ desiccant in each bag to minimize the penetration of ambient humidity. EXAFS data were also collected for a liquid sample of 0.05 M $UO_2(NO_3)_2$ at pH = 2. Under these conditions, the uranyl speciation is predicted to be 92% UO_2^{2+} and 6% $UO_2NO_3^+$.

Data analysis. EXAFS. The reduction and analysis of EXAFS data followed standard practices, using the EXAFSPAK software suite developed at SSRL by G. George and I. Pickering. Oscillatory $\chi(k)$ curves were calculated from the mesured spectra assuming an ionization potential E_0 = 17,181 eV. Structural parameters were extracted from the data by *least-squares* fitting of the k^3-weighted $\chi(k)$ curves. For the transmission-mode data, the fitted range of k-values was 3–16.5 Å^{-1} (3–13.5 Å^{-1} for the aqueous sample). For the fluorescence-mode data, the range was 3–13 or 14 Å^{-1}. The fitting model included at least two coordination shells of O atoms and, in some cases, a single shell of U atoms. Photoelectron scattering amplitudes and phase shifts were calculated using the FEFF 6 code (Rehr *et al.*, 1991). This *ab initio* source of scattering parameters was successfully applied to uranium L_3 EXAFS (Waite *et al.*, 1994; Allen *et al.*, 1995, 1996a, 1996b; Hudson *et al.*, 1996) and XANES (Hudson *et al.*, 1995, 1996). The model compound for the calculation was α-$UO_2(OH)_2$, using atomic coordinates determined by XRD (Taylor, 1971). The axial O atoms of the uranyl cation have different scattering parameters compared to those of the equatorial O atoms. Multiple-scattering (MS) of the photoelectron within the linear uranyl cation influences the EXAFS (Hudson *et al.*, 1996). Contributions from the most important MS path, as determined by FEFF 6, were included in the fits, with the effective bond distance and Debye-Waller (DW) factor both fixed at twice the single-scattering values (*i.e.*, from the axial O shell).

The equatorial atoms around the uranyl cation were assumed to be O, representing possible ligation by water, hydroxide, carbonate, and/or surface O atoms. All data sets were fit twice, by assuming either one or two shells of equatorial O atoms, each with adjustable parameters. An important qualitative result of this analysis is to determine if two equatorial shells are required to best fit a given data set. Due to fundamental limitations, two distinct equatorial shells can be identified only if their U-O bond distances differ by more than the inherent distance resolution of the measurement. For our EXAFS results, this resolution ranges from 0.095 to 0.12 Å, depending on the range of k measured. Smaller differences (splittings) within the equatorial shell cannot be observed directly, although they may become apparent by an increased DW factor, σ^2.

Fits using two equatorial shells which gave apparent splittings less than the resolution were rejected as not physically reasonable. Aside from this restriction, the results based upon the fit with the smaller reduced error are reported here. Note that the reduced error accounts for the introduction of additional adjustable parameters in the fits with two equatorial shells. For all data sets, the statistical indication of a better fit was accompanied by a discernible improvement in the agreement between fit and experiment.

Identifying the presence and degree of splitting in the equatorial shell is one of the most useful results of this EXAFS analysis. Such distortions are sensitive indicators of the chemical interaction between uranyl and the mineral substrate. For example, a split equatorial shell was identified, using EXAFS, for the case of uranyl inner-sphere surface complexation by ferrihydrite (Waite *et al.*, 1994). In that study, the proposed structure was confirmed by identifying a neighboring iron atom at the expected distance. Further evidence for an inner-sphere mechanism came from the application of a surface complexation model to extensive uptake data.

EXAFS features which are indicative of U scatterers were observed for several samples. Fits of possible U features were only undertaken if the corresponding Fourier transform (FT) peak was above the noise level measured at higher $R + \Delta$. The identity of the U scatterer was first confirmed by back-transforming the peak and fitting this Fourier-filtered experimental EXAFS with calculated U parameters. Good agreement was obtained using reasonable values for the U fitting parameters, whereas much poorer agreement and/or unreasonable results were obtained when oxygen or silicon scattering parameters were used.

Because E_0 is closely correlated with interatomic distance R in the fits, the ΔE_0 values for all oxygen shells were fixed at 0 eV. This was very close to the optimum value for most samples. This restriction, which is reasonable for systems with similar chemistry, enhances the significance of trends in the derived bond distances. ΔE_0 was allowed to vary for the U scatterers. Note that the coordination number, N, is closely correlated to the DW factor, and therefore

https://doi.org/10.1346/CCMN.1999.0470406 Published online by Cambridge University Press

Table 3. Mineral characteristics.

Mineral	Surface area (m^2 g^{-1}) <45 μm fraction	Surface area (m^2 g^{-1}) 45–250 μm fraction	CEC (ceq kg^{-1})
Vermiculite	9.03 ± 0.04	1.07 ± 0.01	150.7 ± 0.6
Hydrobiotite	13.4 ± 0.1	1.18 ± 0.01	95.7 ± 1.2

trends in these two parameters should be interpreted carefully.

XANES. The raw XANES spectra were normalized to facilitate comparisons. The pre-edge region was first fitted using either a linear function or $y = a + bx^{-1}$. This function was subtracted from the spectrum. Next, a linear fit to the above-edge region was extrapolated to the E_0 energy, providing a normalization constant. This approach yields an edge jump normalized to unity, with minimal influence from the near-edge fine structure.

RESULTS AND DISCUSSION

Mineral characterization

Results of BET analysis and CEC measurements are listed in Table 3. Using EDS, the vermiculite was found to contain O, Mg, Al, Si, and Fe. The hydrobiotite also contains these elements, as well as K and trace amounts of Ti and Cr. Scanning EDS measurements indicated a homogenous Fe distribution for both minerals, with a spatial resolution of <0.1 μm. All these results are consistent with expectations for these minerals.

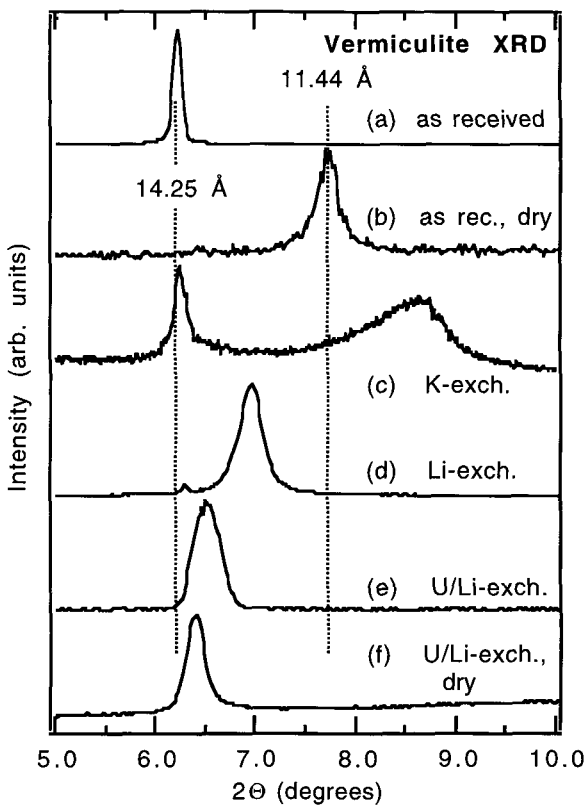


Figure 1. XRD patterns for vermiculite, at ambient humidity except as noted. (a) Mineral as received, (b) Dehydrated, (c) K^+ exchanged, (d) Li^+ exchanged, (e) UO_2^{2+} and Li^+ exchanged, (f) UO_2^{2+} and Li^+ exchanged, dehydrated.

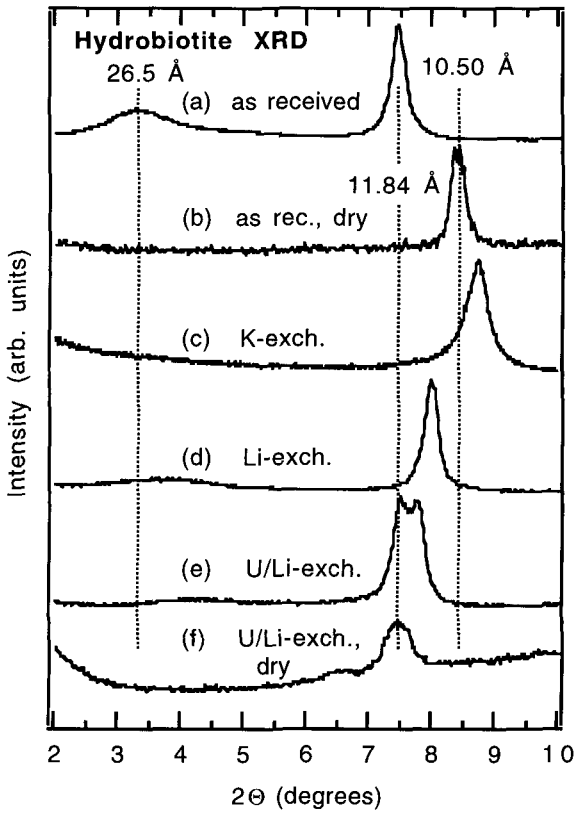


Figure 2. XRD patterns hydrobiotite, at ambient humidity except as noted. (a) Mineral as received. (b) Dehydrated, (c) K^+ exchanged, (d) Li^+ exchanged, (e) UO_2^{2+} and Li^+ exchanged, (f) UO_2^{2+} and Li^+ exchanged, dehydrated.

X-ray diffraction

The XRD results provide a direct measurement of the interlayer spacing $d(001)$. For the expandable layer silicates used here, variation in this distance is indicative of hydration changes or interlayer cation exchange. The results, presented in Figures 1 and 2 and in Table 4, confirm the identification of the minerals and trace the changes occurring during the treatments described above.

Vermiculite. Powder XRD of vermiculite gave results consistent with published vermiculite patterns (Bayliss *et al.*, 1986) and indicated a trioctahedral structure with Mg^{2+} as the predominant interlayer cation. A small amount of chlorite (estimated from peak intensities at <5%) was present in the vermiculite.

https://doi.org/10.1346/CCMN.1999.0470406 Published online by Cambridge University Press

Table 4. Measured XRD spacings.

Treatment	$d(00l)$ (Å)[1]	
	Vermiculite	Hydrobiotite[2]
as received	14.25	27, 11.82, 8.39, 4.92, 3.47, 3.10, 2.69 l = 1, 2, 3, 5, 7, 8, 9
as received, dried	11.41	10.53, (7.05), (5.27), 4.11, 3.41, 3.11, 2.67 l = 2, 3, 4, 5, 6, 7, 8
K^+-exchanged	14.18, 10.2	10.1, 5.02, 3.37, 2.52 l = 1, 2, 3, 4
Li^+-exchanged	(14.09), 12.73	24, 11.06, 5.48, 3.62, 3.20, 2.74, (2.48) l = 1, 2, 4, 6, 7, 8, 9
U/Li^+-exchanged[3]	13.63	20.5, 11.81, 11.39, 8.02, 7.70, 4.80, 3.45, 3.05, 2.70 l = 1, 2a, 2b, 3a, 3b, 5a, 7a, 8a, 9a[4]
U/Li^+-exchanged, dried[5]	13.82	11.88 l = 2

[1] Spacings corresponding to peaks of very low intensity are in parenthesis.

[2] The most likely assignment of diffraction order l is listed for each peak.

[3] Sorption samples V-IE1 and HB-IE1.

[4] These spacings are assigned to two distinct phases, denoted by a and b.

[5] Sorption samples V-IE1-D and HB-IE1-D.

The $d(001)$-value for vermiculite (Figure 1) ranges from ~10 to 15 Å, reflecting changes to the interlayer under various conditions. The untreated vermiculite at ambient humidity has a 14.25-Å spacing, indicative of two water layers in the interlamellar region. For the dried vermiculite, which was not baked, the observed 11.4-Å spacing indicates a single-water-layer structure. The high background in this pattern apparently obscures the chlorite impurity (001) peak at ~14.1 Å. K^+-exchanged vermiculite shows a broad peak at 10.2 Å, indicative of a collapsed interlayer, *i.e.*, a nonhydrated mica-like structure. The 14.2-Å peak persists with considerable intensity, presumably as a result of incomplete K^+-exchange and/or collapse. The considerable asymmetry of the 10.2-Å peak indicates random interstratification of the two spacings. The Li^+-vermiculite, measured at ambient humidity, has a $d(001)$-value of 12.7 Å. In samples saturated with DI water, not shown, this peak nearly disappears and a 14.4-Å peak appears. In dried samples, not shown, the 12.7-Å peak is replaced by a peak at 11.7 Å. These changes with hydration are similar to MacEwan and Wilson (1980).

Sample V-IE1 was prepared by treating Li^+-exchanged vermiculite with uranyl. The XRD results show that uranyl exchange expands the 12.7-Å spacing to 13.6 Å. This is less than the 14.5-Å $d(001)$-value observed for a uranyl-exchanged montmorillonite (Tsunashima *et al.*, 1981). The 13.6-Å spacing is also smaller than the 14.25-Å spacing observed for untreated vermiculite under similar hydration conditions. These comparisons show that the UO_2^{2+} is not behaving as a divalent metal cation. After drying the uranyl/Li^+-vermiculite to obtain sample V-IE1D, the interlayer spacing is essentially unchanged, indicating that water is more tightly bound in the uranyl/Li^+-vermiculite or that the large uranyl cation is hindering reduction of the interlayer. These possibilities are discussed below along with EXAFS and polarized XANES results.

Hydrobiotite. XRD of untreated hydrobiotite showed a $d(001)$-value of ~27 Å and higher-order reflections with spacings and intensities characteristic of regular interstratification (Sawhney, 1967). The pattern resembles that of a Transvaal hydrobiotite (Brindley *et al.*, 1983), with $d(001)$ larger than expected and $d(002)$ somewhat smaller. These comparisons, and the absence of ~10-Å and ~15-Å peaks, indicate that the hydrobiotite used here has almost equal amounts of interstratified biotite and vermiculite layers.

Figure 2 shows results of hydrobiotite exchange reactions that are complicated by the regular interstratification of the layers. The $d(001)$-value ranges from ~20 to ~27 Å and represents the distance between pairs of biotite and vermiculite layers. Because of difficulties in measuring peaks accurately at low angles, and the large width of this peak, this measurement is approximate. Therefore, the much sharper (002) reflection was used for the measurement of spacing changes. Higher-order $d(00l)$-values are reported in Table 4.

The $d(005)$-value confirms that the dry hydrobiotite retained a regular interstratified structure. The (001) peak was not observed for this sample, which was double sealed in 0.10 mm PE bags, apparently due to the large attenuation of X-rays in the plastic at low angles of incidence. After K^+-exchange, the pattern indicates that the vermiculite layer has collapsed and the mineral has adopted a well-ordered mica-like structure with $d(001)$ = 10.1 Å. The three observed higher-order reflections (Table 4) show rational spacings based on the 10.1-Å peak. The absence of a peak at ~20 Å, and of any peaks of l = odd based on the 20-Å peak, demonstrates that interstratification has been eliminated by the collapse of the interlayer associated with the vermiculite layer. In contrast, the Li^+-hydrobiotite shows both a (001) peak at 24 Å and an intense (007) reflection at 3.20 Å, indicating that this form is regularly interstratified.

Sample HB-IE1 was prepared by treating the Li^+-hydrobiotite with uranyl. The resulting XRD pattern (Figure 2e) resolves two (002) reflections, with increased spacings relative to Li^+-hydrobiotite, indicating the presence of two phases with slightly different interlayer spacings. Higher-order peaks are also observed, including odd-order reflections which show

https://doi.org/10.1346/CCMN.1999.0470406 Published online by Cambridge University Press

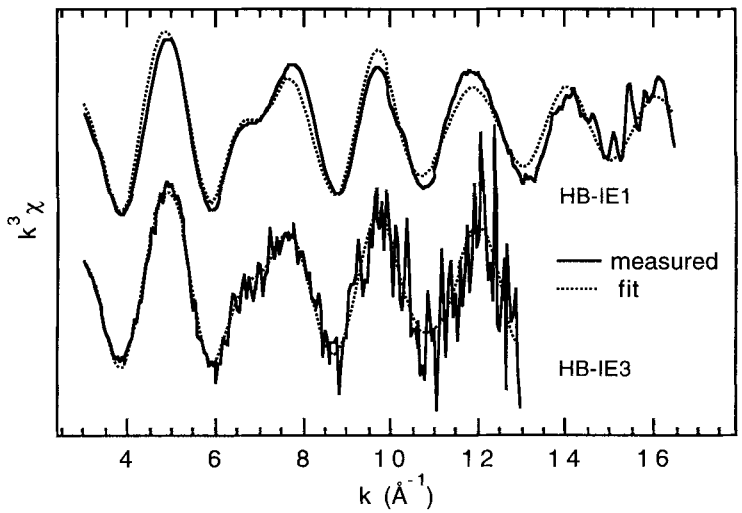


Figure 3. Typical uranium L_3 EXAFS results, plotted as k^3-weighted $\chi(k)$ to show the data and fit quality. Note differences in background between the transmission data for sample HB-IE1 and the fluorescence data for HB-IE3.

that this sample is regularly interstratified. Two (003) peaks are observed, whereas for higher l only a single series is seen, based on the phase with larger spacings (Table 4). Thus the latter phase has a more uniform interlayer spacing. Overall, the XRD pattern shows that the d(001)-value of the uranyl-exchanged Li^+-hydrobiotite is smaller than that of the untreated Mg^{2+}-hydrobiotite. For sample HB-IE1D, obtained by drying HB-IE1, the (002) reflection becomes a single peak, corresponding to the larger of the two spacings observed before drying. The (001) reflection is not observed, probably due to the PE bag which enclosed the dried samples. The insensitivity of interlayer spacing to dehydration is similar the vermiculite sample (see above).

EXAFS

The EXAFS samples are divided into two sets:

(1) Samples prepared using the larger size fraction of the minerals were loaded with greater amounts of U and therefore EXAFS was measured in transmission mode. Low pH, relatively high uranyl concentrations, and small concentrations of competing cations ensured that cation exchange was the principal uranyl sorption mechanism for these samples. Figure 3 shows typical data and fit quality for the transmission data sets. Figure 4 presents all the transmission EXAFS results in Fourier transform plots. Results for the free aquo species UO_2^{2+} are also included for comparison. Derived fit parameters are listed in Table 5. The fairly high U content was evident both from the XAS signals for these sorption samples and from the uptakes measured for the -IE2 samples (Table 1).

(2) Samples prepared using the smaller size fraction of the minerals were loaded with less U, as indicated both by XAS signals and uptake measurements. Therefore the more sensitive fluorescence-detection method was required to measure EXAFS. For these samples, pH and background cation concentration were varied to promote either surface complexation by OH at the layer edges or ion exchange at basal plane sites. The smaller particle size provided an increased edge surface area, improving the possibilities for surface complexation. Figure 3 plots the EXAFS for a typical sample, HB-IE3. Due to the lower U concentrations, the fluorescence data sets have smaller signal-to-noise ratios, and cover shorter k ranges, as compared to the transmission data sets. Figure 5 presents all the fluorescence-EXAFS results in Fourier transform plots. Derived fit parameters are listed in Table 6. The coupling of coordination number, N, and the DW factor, α^2, may be greater for these samples.

For all samples, EXAFS results show that the structure of the uranyl cation is preserved. This indicates that U^{6+} is not reduced to U^{4+} under any of the conditions used here.

Transmission samples—ion exchange. Oxygen Shells. Comparison of the derived EXAFS structural parameters in Table 5 shows a remarkable similarity between analogous samples prepared with the two different minerals. For the two -IE1 samples (V-IE1, HB-IE1), the results are nearly identical. Dehydration (-IE1-D samples) causes similar changes for the two minerals. The two -IE2 samples also have nearly identical structures, except that V-IE2 has a larger U-neighbor contribution. The absence of a substrate dependence for the local structure of uranyl at ion-exchange sites indicates that the interstratification and higher local-charge density of hydrobiotite have little influence

https://doi.org/10.1346/CCMN.1999.0470406 Published online by Cambridge University Press

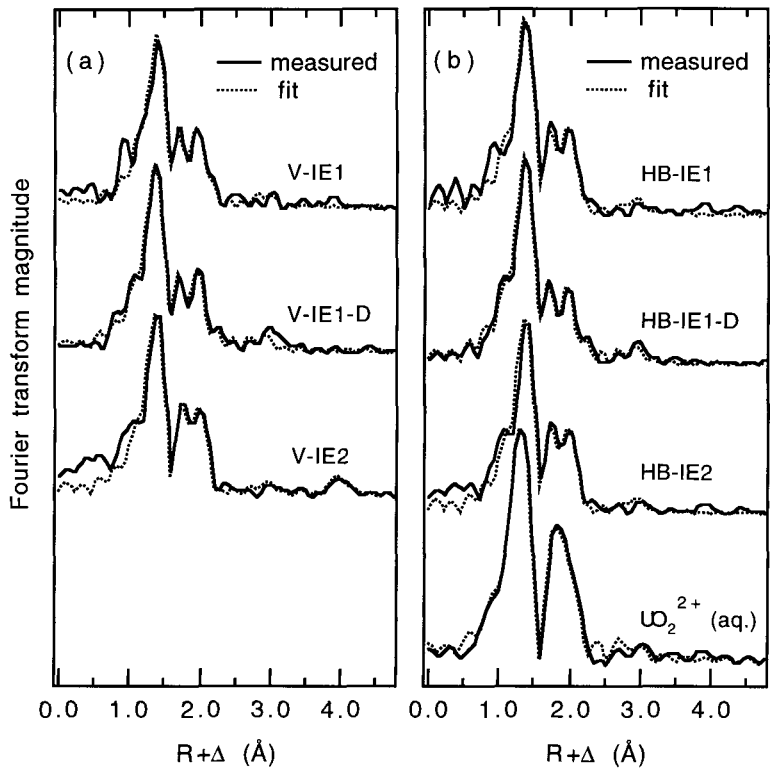


Figure 4. Uranium L_3 transmission EXAFS results for (a) UO_2^{2+}/vermiculite samples and (b) UO_2^{2+}/hydrobiotite samples. The measured curves are plotted as solid lines and the results of *least-squares* fitting are plotted as dotted lines. Note that the apparent interatomic distance for a given peak in the FT includes scattering phase shift, Δ. The actual distance R, as derived by the *least-squares* analysis, is larger.

upon the exchange mechanism. Insensitivity to charge density is also supported by a comparison to U EXAFS studies of uranyl-exchanged smectite clays (Giaquinta *et al.*, 1997). With the low surface-charge smectite substrate, the structural parameters measured for the first two coordination shells are very similar to those obtained here for the -IE1 and -IE2 samples, which used higher surface-charge minerals. The close similarity of the derived -IE1 and IE2 structural parameters indicates that the structure of ion-exchanged uranyl is not influenced by: (1) The different initial interlayer cation (Li^+ *vs.* Mg^{2+}, respectively); or (2) The factor of seventeen difference in the initial solution concentrations of U.

The measured -IE2 U uptakes correspond to significant loading, with a U mass fraction of ~10% for both samples. The large U content arises from extensive ion exchange or possibly from precipitation of a U-bearing phase. At the low pH values used for all the -IE samples, the speciation simulations did not predict precipitation of a bulk U phase. Precipitation can possibly arise from a strong surface interaction, *i.e.*, formation of a surface precipitate. However surface precipitation is unlikely to produce such extensive uptake and is inconsistent with the polarized XANES results discussed below. Thus ion exchange is assumed to be the dominant mechanism for the -IE2 samples and for the structurally similar -IE1 samples.

The results from the UO_2^{2+} aquo complex (Table 5) are similar to the -IE-1 and -IE-2 results. The fairly symmetric equatorial shells derived for the -IE1 and -IE2 structures and their similarity to the uranyl aquo complex structure are strong indications that, for hydrated samples, ion-exchanged uranyl is an outer-sphere complex. A similar conclusion was obtained from U EXAFS measurements for uranyl sorbed to montmorillonite at pH ~ 3.4 (Chisholm-Brause *et al.*, 1994).

Upon dehydration, the ion-exchanged uranyl exhibits similar structural changes for the two minerals, as shown in Table 5 by comparing samples V-IE1 and HB-IE1 to V-IE1-D and HB-IE1-D. The coordination number for the R ~ 2.42-Å shell decreases by ~0.7, and a more distant shell at R ~ 2.56 Å appears with N ~ 0.5–0.7. This probably occurs due to a loss of one coordinating water molecule, which is replaced by a surface O atom at R ~ 2.6 Å. A progression from outer- to inner-sphere structures was previously identified in the dehydration of Mg^{2+}-vermiculites (MacEwan and Wilson, 1980). Regardless of interpre-

https://doi.org/10.1346/CCMN.1999.0470406 Published online by Cambridge University Press

Table 5. EXAFS results, for samples measured in transmission mode. ΔE_o was fixed at 0 eV for all shells, except as noted.

Sample	Shell[1]	N	R (Å)	σ^2 (Å^2)
V-IE1	O_{ax}	2.06	1.78	0.0018
	O_{eq}	4.55	2.43	0.0079
V-IE1-D	O_{ax}	2.02	1.77	0.0017
	O_{eq1}	3.83	2.42	0.0064
	O_{eq2}	0.72	2.57	0.0014
	$O_{eq,av}$		2.44[2]	
V-IE2	O_{ax}	2.11	1.79	0.0021
	O_{eq}	4.87	2.42	0.0075
	U[3]	0.65	4.23	0.0035
HB-IE1	O_{ax}	2.10	1.78	0.0019
	O_{eq}	4.77	2.43	0.0083
HB-IE1-D	O_{ax}	2.09	1.77	0.0016
	O_{eq1}	4.09	2.42	0.0082
	O_{eq2}	0.47	2.56	0.0015
	$O_{eq,av}$		2.43[2]	
HB-IE2	O_{ax}	2.08	1.79	0.0019
	O_{eq}	4.68	2.43	0.0082
UO_2^{2+} (aq.)	O_{ax}	2.39	1.76	0.0028
	O_{eq}	4.84	2.40	0.0068

[1] O_{ax} refers to the axial O shell, O_{eq} refers to the equatorial O shell or shells.

[2] The R value listed for $O_{eq,av}$ is the average R for the equatorial shell, using the derived N values as weighting factors.

[3] $\Delta E_o = -16.7$ eV. A fit to Fourier-filtered U signal gave $N = 0.30$, $R = 4.26$ Å, $\sigma^2 = 0.0021$ Å^2 and $\Delta E_0 = -1.5$ eV.

Table 6. EXAFS results, for samples measured in fluorescence mode. ΔE_o was fixed at 0 eV for all shells, except as noted.

Sample	Shell[1]	N	R (Å)	σ^2 (Å^2)
V-IE3	O_{ax}	2.69	1.77	0.0034
	O_{eq}	3.52	2.43	0.0090
V-SC	O_{ax}	2.23	1.80	0.0032
	O_{eq1}	3.09	2.28	0.0115
	O_{eq2}	1.02	2.48	0.0023
	U[2]	0.63	3.88	0.0023
	$O_{eq,av}$		2.32[3]	
V-SCK	O_{ax}	2.30	1.78	0.0024
	O_{eq}	4.24	2.38	0.0129
HB-IE3	O_{ax}	2.03	1.78	0.0012
	O_{eq1}	3.76	2.39	0.0087
	O_{eq2}	0.90	2.51	0.0002
	$O_{eq,av}$		2.41[3]	
HB-SC	O_{ax}	2.10	1.79	0.0012
	O_{eq1}	1.27	2.24	0.0076
	O_{eq2}	3.09	2.42	0.0060
	$O_{eq,av}$		2.37[3]	
HB-SCK	O_{ax}	2.73	1.80	0.0035
	O_{eq1}	2.87	2.24	0.0125
	O_{eq2}	1.85	2.44	0.0055
	U[4]	0.43	3.90	0.0012
	$O_{eq,av}$		2.32[3]	

[1] O_{ax} refers to the axial O shell, O_{eq} refers to the equatorial O shell or shells.

[2] $\Delta E_o = +0.6$ eV. A fit to Fourier-filtered U signal gave $N = 0.71$, $R = 3.91$ Å, $\sigma^2 = 0.0043$ Å^2 and $\Delta E_0 = +4.0$ eV.

[3] The R value listed for $O_{eq,av}$ is the average R for the equatorial shell, using the derived N values as weighting factors.

[4] $\Delta E_o = +0.5$ eV. A fit to Fourier-filtered U signal gave $N = 0.94$, $R = 3.89$ Å, $\sigma^2 = 0.0047$ Å^2 and $\Delta E_0 = -0.7$ eV.

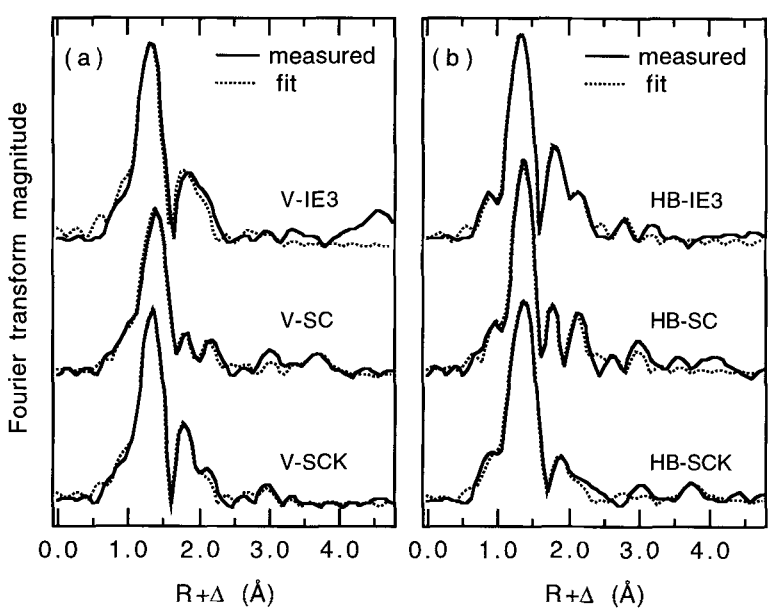


Figure 5. Uranium L_3 fluorescence EXAFS results for (a) UO_2^{2+}/vermiculite samples and (b) UO_2^{2+}/hydrobiotite samples. See Figure 4 for details.

https://doi.org/10.1346/CCMN.1999.0470406 Published online by Cambridge University Press

tation, a modification of the equatorial shell upon dehydration is clearly shown by the EXAFS results. This is direct evidence of a local structural change for the two dried samples under conditions which did not induce an interlayer contraction, as observed by XRD. These results indicate that some water is removed from the interlamellar region at low humidity, but contraction is hindered, perhaps by steric effects of the uranyl cation.

Additional Shells. The EXAFS FT in Figure 4a for sample V-IE1-D, which has a good signal-to-noise ratio, shows indications of a neighboring atom contributing FT magnitude at $R + \Delta \sim 3.1$ Å. Analysis of potential neighbors in this interatomic distance range is complicated by multiple-scattering (MS) contributions, including those from the uranyl axial O atoms. The approach used here is to fit the Fourier-filtered EXAFS from this range with a combination of axial MS and single scattering from a neighboring atom. For this data set, the filtered signal could not be successfully fit with reasonable structural parameters when the neighboring atom was assumed to be Si, O, or U. Note that electron scattering parameters vary gradually with atomic number, so Si serves also as a model for Al and Mg. The lack of success in this case may indicate that the measured FT has a spurious peak, or that interfering signals from several different neighbors at similar distances create the feature. The limited success of uranyl MS modeling by FEFF 6, which has been previously discussed (Hudson, *et al.* 1996), may also prevent an accurate analysis of the filtered signal. No definitive conclusion is possible at present, although the presence of a scatterer in this distance range is consistent with the formation of an inner-sphere complex, as proposed above.

In Figure 4a, sample V-IE2 shows a FT peak, well above noise levels, which is assigned to a U shell at $R \sim 4.2$ Å. The large ΔE_0 value obtained for this shell in the full EXAFS analysis is not physically meaningful. However the value obtained in the fit to the Fourier-filtered U peak is more reasonable (Table 5). This fit to the V-IE2 filtered U signal is not as successful as the fit shown below for V-SC, with some phase and amplitude disagreement for $k < 6$ Å^{-1}. However the overall agreement is worse, and fit parameters became unreasonable, if Si or O scatterers were assumed instead. The FT's of samples V-IE1, HB-IE1, and HB-IE2, in Figure 4, show a possible U feature at $R + \Delta \sim 3.9$ Å, with less magnitude than the corresponding feature for V-IE2. Fits to the filtered peaks, not presented here, gave results similar to those for V-IE2, with smaller coordination numbers and ΔE_0 between -9 and -15 eV. Overall the results for V-IE2 are more compelling evidence of U neighbors, because they are based upon a larger-magnitude experimental feature. Samples V-IE1-D and HB-IE1-D show no indication of U neighbors.

Solution conditions for the transmission samples were well below solubility limits for any known U bulk phase. The observed U-U distance of ~4.2–4.3 Å is too large to result from a reported di-hydroxyl-bridged uranyl dimer structure. EXAFS measurements yielded a U-U distance of ~3.9 Å for several such dimers (Allen *et al.*, 1996a). Furthermore, the equatorial bond distances derived here are different from those observed for such dimers. The present results suggest a tendency for outer-sphere uranyl at ion-exchange sites to form loosely bound oligomers. The derived U-U distance suggests dimers which share a single equatorial ligand, though the direct observation of a fairly uniform equatorial O shell, without splitting, appears to contradict this model. Perhaps dimers are favored by the structured aqueous environment of the interlayer region rather than by a direct bonding between uranyl complexes. Dehydration could alter this environment, leading to the observed absence of the U neighbor for V-IE-D and HB-IE-D. Note that surface precipitation is not a likely explanation for the presence of a U neighbor, based on the preceding discussion and the polarized XANES results given below. Also disappearance of the U neighbor upon dehydration is difficult to reconcile for a surface precipitate.

Fluorescence samples—ion exchange vs. sorption by surface hydroxyls. Oxygen Shells. Structural parameters derived from the *least-squares* analysis are presented in Table 6. Results for sample HB-IE3 are similar to those of HB-IE1-D, with a split equatorial shell of about four O atoms at an intermediate distance and a more distant O atom. Results for the analogous sample V-IE3 indicate a single equatorial shell at the same distance observed for other ion-exchange samples. Although stable fits with two resolved equatorial shells were not obtained for V-IE3, note in Figure 5a that the fit may be missing a scattering shell around $R + \Delta \sim 2.1$ Å. Therefore, V-IE3 may be structurally more similar to HB-IE3 than the listed fit parameters suggest. In any case, the split-shell result for HB-IE3 probably reflects the much lower U content, as compared to the other HB ion-exchange samples. At lower loadings, a significant portion of the uranyl may bond at defect and/or impurity sites which are chemically reactive but present in low concentrations in the mineral. Defects are expected to be more common in more finely ground -IE3 powders, as compared to other -IE samples. The formation of strong bonds to these chemically active sites would create inner-sphere complexes with split equatorial shells, as observed for HB-IE3. Alternatively, the results for HB-IE3 may be realted to the much larger surface area of this sample, as compared to the other HB ion-exchange samples. This sample should have a greater fraction of uranyl bound

https://doi.org/10.1346/CCMN.1999.0470406 Published online by Cambridge University Press

to ion-exchange sites on *external* basal plane surfaces, as opposed to interlamellar surfaces. Uranyl at these external sites does not have the symmetric environment of two closely separated surfaces, and the measured distortion of the equatorial shell may reflect a more directional, possibly inner-shell, interaction with the single basal plane surface.

The -SC samples for both vermiculite and hydrobiotite exhibit a large splitting of the equatorial shell, with a difference in bond distance of 0.18–0.20 Å. The average axial bond distance for all ion-exchange samples is 1.78 Å, whereas the two -SC samples have larger values of 1.80 and 1.79 Å. This is probably a significant difference, which indicates stronger overall *equatorial* chemical bonding to the U for the -SC samples. A similar conclusion is obtained by comparing the averaged equatorial bond distances (Tables 5 and 6). These are smaller for all the -SC and -SCK samples, as compared to all the -IE samples.

This trend towards stronger overall equatorial bonding, and especially the pronounced equatorial splitting, is consistent with several possible sorption mechanisms, all involving hydrolysis or similar processes. One possibility is bidentate, monomeric inner-sphere surface complexation, where the splitting of the equatorial groups arises because the two surface O atoms are more distant from the U than the other equatorial O atoms. Another possibility is the presence of aqueous uranyl species, such as hydroxyl and carbonate complexes, bound as inner-or outer-sphere complexes on the mineral surface. Uranyl is predicted to form a variety of monomeric and oligomeric aqueous complexes under the near-neutral pH conditions used here (Table 2). Molecular structures are not well known for these complexes, but it is likely that they would exhibit a split equatorial shell, due to the combination of strong ligands (OH^-, CO_3^{2-}) and weak ligands (H_2O). On surfaces, such complexes could exhibit equatorial splitting as a result of complexation by free ligands, regardless of surface interaction. A third possibility is the formation, through hydrolysis reactions, of a precipitate or surface precipitate. Uranyl in such solids will also exhibit a split equatorial shell. These possibilities are considered in more detail below. Regardless of interpretation, the EXAFS measurements clearly indicate that the local structure of uranyl is modified under conditions which favor sorption at surface hydroxyl sites, as compared to ion exchange sites.

Two U EXAFS studies of uranyl sorbed on montmorillonite at near-neutral pH (Dent *et al.*, 1992; Chisholm-Brause *et al.*, 1994) gave results similar to those observed here. Although splitting of the equatorial shell was not resolved due to the limited *k*-range of the data sets, both studies indicated a large amount of static disorder in the equatorial shell. Using U EXAFS, a significant splitting of the equatorial shell was observed for uranyl sorbed on ferrihydrite (Waite *et al.*, 1994). That local structure was attributed to bidentate, monomeric inner-sphere surface complexation, as discussed in the data analysis section above.

The -SCK samples were prepared by exposing uranyl to K^+-exchanged minerals with collapsed interlayer regions. These samples were used to assess whether the interlayer regions play an active role in sorption under the conditions intended to favor sorption at layer edge sites. The derived bond lengths for HB-SCK are very similar to those of HB-SC, suggesting similar chemistry. This suggests that interlayer ion-exchange is not the dominant process under these conditions.

In contrast, the structural parameters for V-SCK are not similar to those from V-SC. The single equatorial shell and the axial bond length of 1.78 Å are similar to results for the ion-exchanged V-IE samples, but the equatorial bond distance is smaller. Note that the XRD results indicated only partial interlayer collapse for the K^+-vermiculite. This may explain the difference in EXAFS results for V-SCK, as compared to HB-SCK, which had complete collapse. However it is not clear why incomplete collapse would lead to the observed structure. One possibility is that the vermiculite ion exchange sites are highly selective for cationic uranyl species over the monovalent K cations, leading to significant ion exchange of uranyl for K^+ within the non-collapsed interlayer. For cation exchange on montmorillonite, UO_2^{2+} was found to be highly preferred to K^+, especially at low uranyl concentrations (Tsunashima *et al.*, 1981). However the aqueous UO_2^{2+} concentration for V-SCK is predicted to be four orders of magnitude less than the K^+ concentration, and the UO_2OH^+ concentration is expected to be three orders of magnitude less. Even highly preferential exchange chemistry may be unable to overcome the K^+ mass action advantage.

Additional Shells. A U shell was included in the fit for samples V-SC and HB-SCK. The identification of U is confirmed by the fit to the Fourier filtered signal (Figure 6 for the V-SC data). Excellent agreement between the calculated and filtered EXAFS is obtained using reasonable fit parameters (Table 6). Similar results were obtained for the filtered HB-SCK data. Attempts to fit the filtered EXAFS with Si or O scatterers gave much poorer agreement and unreasonable parameters. Due to high noise, we cannot determine if an appreciable U-U contribution is present for samples V-IE3, HB-IE3, or HB-SC. However, sample V-SCK has lower noise, and shows no indication of a U neighbor. Thus, the U shell observed for V-SC is absent for V-SCK, a difference which is not surprising in light of the dissimilar equatorial structures discussed above.

For the two samples with a clear U-U contribution, V-SC and HB-SCK, we believe at least part of that signal arises from an oligomeric surface species and/or a surface precipitate. Other possible origins exist.

https://doi.org/10.1346/CCMN.1999.0470406 Published online by Cambridge University Press

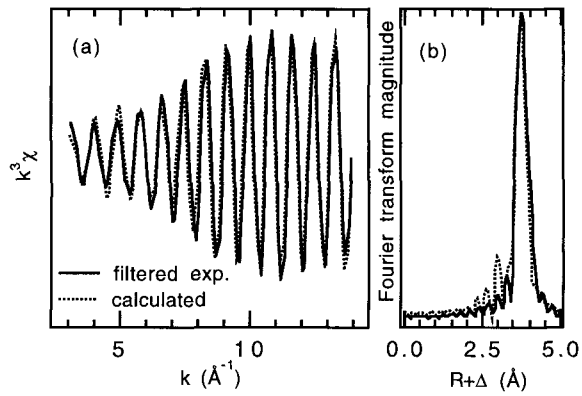


Figure 6. Fourier-filtered EXAFS showing a neighboring U atom at ~3.9 Å. (a) k^3-weighted $\chi(k)$ curves, (b) Fourier transforms of k^3-weighted $\chi(k)$ curves. The solid line is the filtered data for sample V-SC and the dotted line is the fit, using U scattering parameters. The high quality of the fit indicates that this neighbor is indeed a U atom.

In particular, speciation calculations for the -SC and -SCK samples indicate possible bulk schoepite or soddyite precipitation. Fortunately U EXAFS measurements are available for both of these phases, allowing direct comparisons.

For soddyite, a single uranyl equatorial shell was observed in two studies, with reported values of R = 2.38 Å (Reich *et al.*, 1996) and R = 2.36 Å (Farges *et al.*, 1992). This equatorial structure is different from any observed here, except for V-SCK. However results for V-SCK indicated the *absence* of a U neighbor, whereas a U shell was observed for soddyite at R ~ 3.9 Å (Reich *et al.*, 1996). We therefore conclude that soddyite did not form in any sample.

EXAFS results for schoepite indicate an axial shell at R = 1.80 Å and a split equatorial shell with bond distances 2.26 and 2.47 Å (Allen *et al.*, 1996b). This structure is in agreement with the derived parameters for HB-SC, HB-SCK, and especially V-SC. In addition, a U shell was reported for schoepite at 3.84 Å (Allen *et al.*, 1996b). A U shell was observed at about this distance for V-SC and HB-SCK. However, a comparison of the U signal strength shows that the U-U contribution to the EXAFS in schoepite is about twice the contribution observed for V-SC or HB-SCK, or for the maximum possible contribution from HB-SC. To avoid error from the correlation between derived coordination number and DW factor, these comparisons are based upon the integrated EXAFS amplitude

$$N \int \exp(-2k^2\sigma^2)\, dk \qquad (1)$$

taken over the same k range. This comparison suggests that a schoepite phase may account for some, but not all, of the U in samples V-SC, HB-SCK, and possibly HB-SC. Therefore uranyl may be present as a heterogeneous mixture of bulk schoepite and a surface species lacking an ordered U neighbor shell, *e.g.*, a monomeric species.

The reduced U signal, relative to schoepite, may alternatively be attributed to the predominance of an amorphous schoepite-like phase. Static disorder in such a phase may significantly reduce the EXAFS signal from the U neighbor shell. EXAFS measurements on an amorphous hydrous uranyl oxide (Dent *et al.*, 1992) showed a U shell at 3.9 Å with an integrated amplitude similar to that measured here for V-SC and HB-SCK. A disordered phase would be less stable and thus have a higher solubility than well-ordered schoepite. Therefore a disordered phase would not be expected to precipitate in bulk at concentrations near the schoepite solubility, as used here. However, the amorphous phase may stabilize by bonding to the mineral surface, leading to a surface precipitate rather than a bulk phase. In fact, a disordered precipitate is kinetically favored over the direct precipitation of well-ordered schoepite. Comparable behavior is observed in the hydrolysis of Fe^{3+}, where amorphous $Fe(OH)_3$ precipitates from alkaline solutions, and then slowly transforms to more stable crystalline phases α-FeO(OH) and α-Fe_2O_3 (Baes and Mesmer, 1976). Thus a second, more likely, interpretation of the EXAFS results is that an amorphous schoepite-like surface precipitate formed on samples V-SC and HB-SCK.

Another potential origin for the observed U shell in V-SC and HB-SCK is the formation of oligomeric uranyl structures. Although the U interatomic distance derived here is similar to that found for di-hydroxyl-bridged uranyl dimers (Allen *et al.*, 1996a), the equatorial structure is different. The dimers have equatorial bond distances of ~2.34 and 2.46 Å, a poor match to our samples. Although this structure might not be present, some other oligomeric uranyl surface species may exist in our samples, especially because of the aqueous phase speciation, which may include appreciable amounts of $(UO_2)_2CO_3(OH)_3^-$ and possibly $(UO_2)_3(OH)_5^+$ (Table 2). Therefore a third interpretation of the results is that the U neighbor shell arises from oligomeric uranyl surface species in samples V-SC and HB-SCK. Of these three interpretations, a surface precipitate or surface oligomers appear to be most plausible, and these two possibilities may result from similar surface interactions. Both interpretations are consistent with the results for equatorial structure discussed above.

Around $R + \Delta \sim 3$ Å, samples V-SC and HB-SC show FT magnitude above background which is not reproduced in the fitted curve, possibly indicating the presence of a neighboring atom. As described above for sample V-IE1-D, EXAFS analysis at this distance is complicated by the MS contributions from uranyl. Attempts to fit the Fourier filtered signal by a combination of MS and a shell of O, Si, or U were unsuc-

https://doi.org/10.1346/CCMN.1999.0470406 Published online by Cambridge University Press

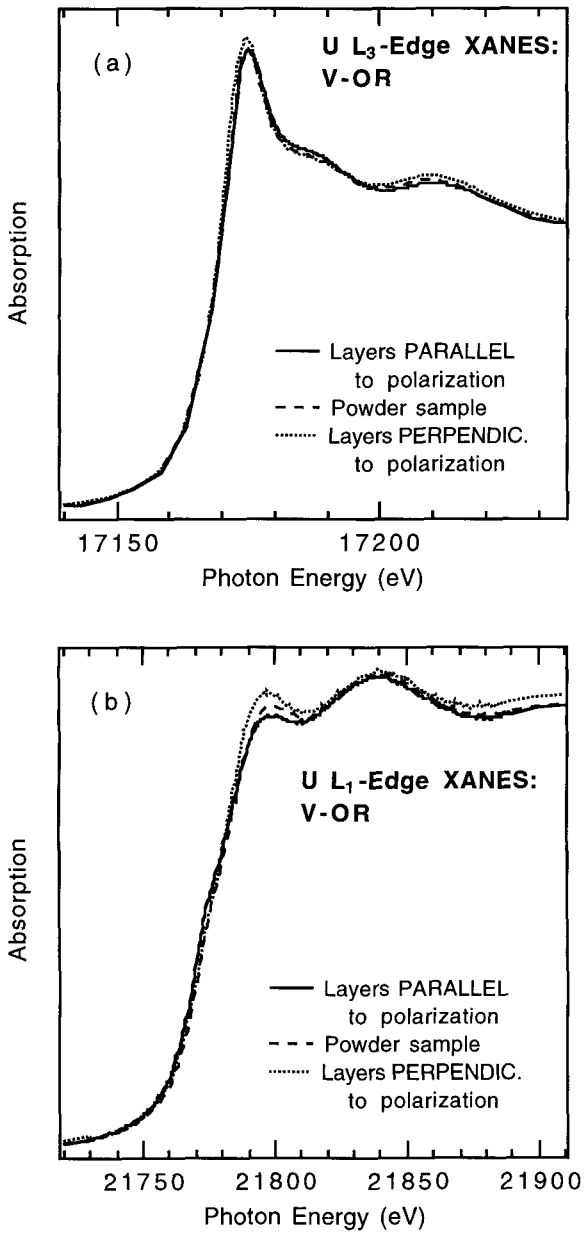


Figure 7. Polarization dependence of U XANES spectra for vermiculite V-OR. (a) L_3 XANES, (b) L_1 XANES. The solid and dotted lines represent spectra measured with the mineral layers parallel or perpendicular to the X-ray polarization vector, respectively. XANES spectra from sample V-IE1 are plotted as dashed lines; this powder sample was prepared under conditions nearly identical to those used for V-OR. The spectral trends indicate that the uranyl cation is preferentially oriented parallel to the layers.

cessful for both data sets. However, an ordered shell of atoms is possible at this distance. In fact, due to high noise levels, such neighbors are a possibility for any of the fluorescence samples. Note that a neighboring atom in this distance range was identified as Fe using uranium EXAFS (Waite *et al.*, 1994) but this is more difficult for an analogous Si, Mg, or Al atom, due to their smaller electron scattering amplitudes.

Polarized XANES

The uranium L_3 and L_1 XANES of the uranyl cation display striking variations depending upon the orientation of the X-ray plane-polarization vector either parallel or perpendicular to the uranyl axis (Templeton and Templeton, 1982; Hudson *et al.*, 1996). The polarization dependence is used here to measure the orientation of uranyl cations sorbed in the interlayer of vermiculite and hydrobiotite. This measurement requires a sample with a well-defined orientation of (basal) planes, obtained here by cutting slices from a well-formed crystal. Figure 7 shows the polarized XANES results for sample V-OR. Besides measurements with the polarization either parallel or perpendicular to the mineral layers, the corresponding measurements for powder sample V-IE1 are also plotted for the non-oriented case. These samples were prepared under similar conditions, and differences in the spectra are primarily due to polarization effects.

Figure 7a compares the uranium L_3 XANES spectra. A small variation is observed, such that the white line maximum at ~17,175 eV and the above-edge resonance at ~17,208 eV are more intense, and the resonance at ~17,187 eV is less intense, when the polarization is perpendicular to the layers. This trend indicates a preferred orientation of the uranyl axis parallel to the layers. Specifically, these results show that there is a distribution of uranyl orientations which, overall, favors directions closer to parallel than to perpendicular alignment. Similarly, the uranium L_1 XANES spectra (Figure 7b) show variations indicative of a preferred orientation of uranyl parallel to the layers. Note that the powder spectrum is intermediate to the two polarized spectra at both the L_3 and L_1 edges, as expected. Figure 8 presents similar spectra for analogous samples HB-OR and HB-IE1. Again, a preferential orientation of uranyl parallel to the layers is observed.

The observation that the uranyl axis is preferentially oriented parallel to the layers is strong evidence that uranyl is mostly sorbed in the interlayer, as expected for exposure conditions that favor ion exchange. Other possible mechanisms for U retention, *i.e.*, edge-site sorption by complexation or by surface precipitation, are less likely to produce a preferred orientation. The EXAFS results for the corresponding powder samples were suggestive of an outer-sphere complex. Therefore the preferred orientation of uranyl observed here is likely a result of steric effects rather than a direct surface bond. Apparently, the stacking requirements of the interlayer hold the uranyl parallel to the layers. EXAFS results for V-IE1 and HB-IE1 also indicated the possible presence of a neighboring U atom. This

https://doi.org/10.1346/CCMN.1999.0470406 Published online by Cambridge University Press

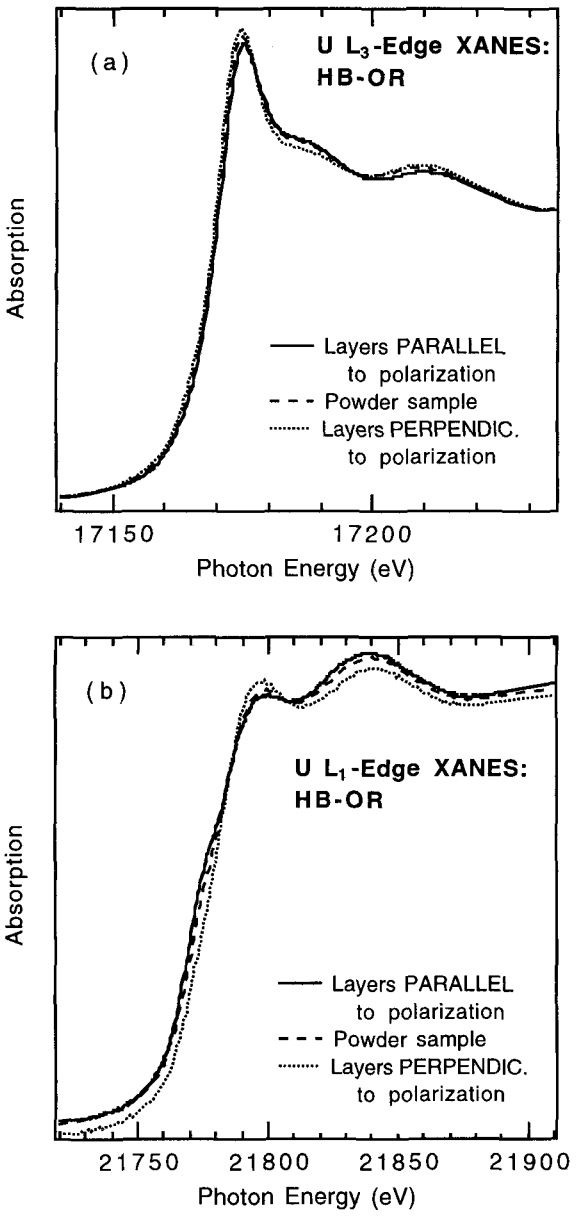


Figure 8. Polarization dependence of U XANES spectra for hydrobiotite sample HB-OR. See Figure 7 for details. Spectra from sample HB-IE1 are plotted as dashed lines; this powder sample was prepared under conditions nearly identical to those used for HB-OR. The spectral trends indicate that the uranyl cation is preferentially oriented parallel to the layers.

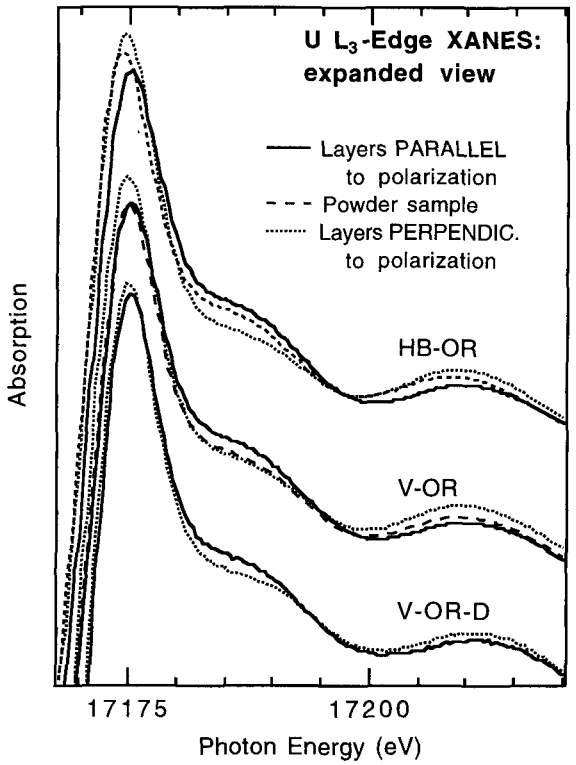


Figure 9. Expanded views of the uranium L_3 XANES polarization dependence. The HB-OR and V-OR data is taken from Figures 7a and 8a. Also shown are L_3 XANES spectra for the dried vermiculite sample V-OR-D. The comparison shows that the orientation effect is smallest in the dried sample, V-OR-D.

weak U-U interaction could also contribute to the observed orientation of uranyl.

Figure 9 shows the uranium L_3 XANES spectra for the dried sample V-OR-D and the uranium L_3 XANES spectra from Figures 7 and 8 for comparison. Note that the corresponding spectrum for powder sample V-IE1-D was not measured with the same spectral resolution and thus cannot be compared to V-OR-D. The L_3-edge polarization dependence shows the same trends as the other two oriented samples. The polarization dependence is more distinct in these expanded plots, but is fairly small compared to the full effect, *i.e.*, the effect observed when most uranyl ions are either nearly parallel or perpendicular to the polarization (Hudson *et al.*, 1996). Therefore the orientational ordering in these mineral samples has a mean uranyl direction which is tilted, relative to the layers, and/or a large amount of orientational disorder. Note in Figure 9 that the polarization dependence is largest for HB-OR and smallest for V-OR-D. This trend may arise from greater orientational ordering of the uranyl ions in HB-OR and/or from a mean uranyl orientation more nearly parallel to the layers in HB-OR. In either case, the probable origin for the difference between hydrated hydrobiotite and vermiculite (*i.e.*, HB-OR and V-OR) is the larger negative charge density of the hydrated basal-plane surfaces in hydrobiotite. Apparently the increased Coulombic forces produce a better-ordered interlamellar region and/or a structure in which uranyl is less tilted relative to the layers.

Comparing the polarization dependence for V-OR and V-OR-D in Figure 9, note that drying the sample

https://doi.org/10.1346/CCMN.1999.0470406 Published online by Cambridge University Press

produces a decrease in the preferential orientation of uranyl parallel to the layers. The EXAFS results for the corresponding powder samples suggest that the uranyl in the dried sample is in an inner-sphere complex with a surface O atom. A decrease in orientational order seems unlikely upon formation of a stronger surface bond. Therefore the diminished polarization effect probably results from the inner-sphere complex where the uranyl axis tilts relative to the layers. The direct bond of an inner-sphere complex could induce such a change. An alternative explanation for the reduced orientation is the apparent loss of a U neighbor upon dehydration, as suggested by EXAFS results for the -IE1 and -IE1-D samples. If U-U bonds are contributing, in part, to preferential orientation, the loss of such bonds may reduce the overall observed orientation by reducing orientational order and/or by promoting the tilting of uranyl relative to the layers.

If increased tilting of uranyl is the cause of the diminished orientational order, this suggests an interpretation for the unusual absence of interlayer reduction upon dehydration, which was detected by XRD for the powder samples. As water is removed, the inclination of the uranyl axis increases and steric interactions prevent the contraction of the interlayer. At the least, the EXAFS and polarized XANES results clearly indicate a dehydration-induced change in the U local structure, in contrast to the XRD results which show no apparent effect. This conclusion emphasizes the usefulness of direct probes of molecular structure.

CONCLUSIONS

The combination of modeling and experimental measurements employed for these studies provided a number of notable results. Generally, for all U-mineral samples examined by XAS, the results show the persistence of the uranyl species upon sorption. There is no significant surface reduction of U^{6+} for the conditions studied. Note that analogous uranyl sorption samples prepared from the two minerals generally gave similar XAS and XRD results, especially for conditions favoring ion exchange. This suggests that the trends observed here are typical for uranyl sorption on expandable phyllosilicate minerals.

The close similarity of EXAFS results from the heavily-loaded -IE1 and -IE2 samples indicates that uranyl bound at ion-exchange sites has the same local structure, independent of differences in basal-plane surface charge and initial interlayer cation. This structure shows a uniform equatorial shell of O ligands similar to those of the free uranyl aquo species, suggesting that an outer-sphere ion-exchange mechanism is dominant here. Polarized-XANES results showed that the ion-exchange uranyl is preferentially oriented parallel to the mineral layers. The observation of a U-U separation of $R \sim 4.2$ Å in some or all of the hydrated -IE1 and -IE2 samples is problematic, given solution conditions which favor monomeric aqueous species and equatorial structures not typical of uranyl dimers. One possible explanation is that the structured aqueous environment of the interlayer favors arrangements which force the uranyl species closer together. A more thorough XRD study to determine the U atomic positions for a well-ordered uranyl-exchanged layer silicate would help to interpret the present results.

Dehydrated versions of the -IE1 samples show modifications to the local structure. In particular, the observed equatorial structure is consistent with a monodentate inner-sphere ion-exchange species. Dehydration removes all evidence of U-U association, and reduces the preferential orientation of uranyl parallel to the layers. However XRD measurements do not show the usual decrease in the interlayer spacing upon dehydration, although such dehydration effects are clearly observed in samples which did not contain U. The interpretation is that removal of water from the interlayer promotes the formation of inner-sphere complexes, with a loss of U-U interactions. This modification produces an increased tilting and/or disorder of the uranyl axial orientation, preventing the contraction of the $d(001)$-value. These results may be clarified by a detailed XRD study or by more extensive polarized XANES experiments, which could directly measure the angular disorder.

The -IE3 ion-exchange samples, prepared with much lower U loading, exhibit local structures consistent with formation of inner-sphere complexes. The different bonding, based on U loading, may be the result of sorption at chemically active surface defect sites, or possibly upon external basal-plane surfaces, both of which would be more prevalent in the smaller size fractions used for these samples.

EXAFS results for the -SC samples indicate that, under conditions favoring complexation at amphoteric edge sites, the local environment of bound uranyl differs from ion-exchanged uranyl. Specifically, the equatorial shell shows a pronounced splitting into two bond distances, and trends in the axial and equatorial bond distances indicate stronger overall equatorial bonding. Thus the EXAFS experiment characterized the atomic-level differences between uranyl sorption at two different surface sites. The observed local uranyl structure shows little change between an expanded and collapsed hydrobiotite sample (HB-SC and HB-SCK), indicating that sorption is occurring primarily outside the interlayer. This supports the assumption that conditions used for the -SC samples favor sorption at edge sites. In contrast, the analogous comparison for vermiculite shows notable structural changes. These are most likely due to the incomplete collapse of the K^+-exchanged sample, which was evident from XRD measurements.

Evidence of U neighbors at ~3.9 Å for some of the -SC samples assists in the interpretation of the EXAFS

https://doi.org/10.1346/CCMN.1999.0470406 Published online by Cambridge University Press

results. Of the possibilities considered here, the most likely are: (1) The formation of an amorphous schoepite-like surface precipitate and (2) The sorption of oligomeric uranyl complexes containing hydroxy and/or carbonate ligands from the aqueous phase. A better understanding of uranyl aqueous speciation, in both the thermodynamic modeling and the details of local atomic structure, would allow better characterization of uranyl sorption. In particular, a more accurate determination of the $UO_2(OH)_2$ (aq.) formation constant is essential for an improved understanding of near-neutral pH uranyl aqueous speciation and precipitation.

In summary, the most significant conclusions are: (1) Under low-pH conditions which greatly favor ion-exchange sorption mechanisms, uranyl retains a symmetric local structure suggestive of an outer-sphere complex, with a preferred orientation of the uranyl axis parallel to the mineral layers; (2) Upon dehydration, these ion-exchange complexes adopt a less symmetric structure, consistent with an inner-sphere complex, with less pronounced orientation of the uranyl axis; and (3) For neutral-pH conditions favoring sorption at surface hydroxyl sites, uranyl has a highly distorted equatorial shell, indicative of stronger equatorial ligation. The detection of a neighboring U atom suggests the formation of surface precipitates and/or oligomeric complexes.

ACKNOWLEDGMENTS

The authors thank R. Pletcher of LLNL for expert assistance in the preparation of mineral samples, and J. Woicik for technical support at NSLS. C. Bruton and T. Wolery of LLNL provided useful advice on speciation calculations and access to the EQ3NR code and GEMBOCHS data base. NSLS and SSRL are supported by the U.S. Department of Energy, Divisions of Materials Sciences and Chemical Sciences. This work was supported in part by the Division of Materials Science, Office of Basic Energy Science, and performed under the auspices of the U.S. Department of Energy by Lawrence Livermore National Laboratory under contract W-7405-ENG-48.

REFERENCES

Allen, P.G., Bucher, J.J., Clark, D.L., Edelstein, N.M., Ekberg, S.A., Gohdes, J.W., Hudson, E.A., Kaltsoyannis, N., Lukens, W.W., Neu, M.P., Palmer, P.D., Reich, T., Shuh, D.K., Tait, C.D., and Zwick, B.D. (1995) Multinuclear NMR, Raman, EXAFS, and x-ray diffraction studies of uranyl carbonate complexes in near-neutral aqueous solutions. *Inorganic Chemistry*, **34,** 4797–4807.

Allen, P.G., Shuh, D.K., Bucher, J.J., Edelstein, N.M., Reich, T., Denecke, M.A., and Nitsche, H. (1996a) EXAFS determination of uranium structures: The uranyl ion complexed with tartaric, citric, and malic acids. *Inorganic Chemistry*, **35,** 784–787.

Allen, P.G., Shuh, D.K., Bucher, J.J., Edelstein, N.M., Palmer, C.E.A., Silva, R.J., Nguyen, S.N., Marquez, L.N., and Hudson, E.A. (1996b) EXAFS determination of uranium structures: Schoepite and other U(VI) oxide precipitates. *Radiochimica Acta*, **75,** 47–53.

Baes, C.F., Jr. and Mesmer, R.E. (1976) *The Hydrolysis of Cations*. Wiley, New York, 489 pp.

Bayliss, P., Erd, D.C., Mrose, M.E., Sabina, A.P., and Smith, D.K. (1986) *Mineral Powder Diffraction File Data Book*. International Center for Diffraction Data, Swarthmore, Pennsylvania, USA, 596 pp.

Brindley, G.W., Zalba, P.E., and Bethke, C.M. (1983) Hydrobiotite, a regular 1:1 interstratification of biotite and vermiculite layers. *American Mineralogist*, **68,** 420–425.

Brown, G.E., Jr. (1990) Spectroscopic studies of chemisorption reaction mechanisms at oxide-water Interfaces. In *Reviews in Mineralogy, Volume 23, Mineral-Water Interface Geochemistry*, M.F. Hochella, Jr. and A.F. White, eds., Mineral Society of America, Washington, D.C., 309–363.

Bucher, J.J., Edelstein, N.M., Osborne, K.P., Shuh, D.K., Madden, N., Luke, P., Pehl, D., Cork, C., Malone, D., and Allen, P.G. (1996) A multi-channel Ge detector system for fluorescence x-ray absorption spectroscopy. *Reviews of Scientific Instruments*, **67,** 1–4.

Chisholm-Brause, C., Conradson, S.D., Buscher, C.T., Eller, P.G., and Morris, D.E. (1994) Speciation of uranyl sorbed at multiple binding sites on montmorillonite. *Geochimica et Cosmochimica Acta*, **58,** 3625–3631.

Dent, A.J., Ramsay, J.D.F., and Swanton, S.W. (1992) An EXAFS study of uranyl ion in solution and sorbed onto silica and montmorillonite clay colloids. *Journal of Colloid and Interface Science*, **150,** 45–60.

Farges, F., Ponader, C.W., Calas, G., and Brown, G.E., Jr. (1992) Structural environments of incompatible elements in silicate glass/melt systems: II. U^{IV}, U^{V}, and U^{VI}. *Geochimica et Cosmochimica Acta*, **56,** 4205–4220.

Giaquinta, D.M., Soderholm, L., Yuchs, S.E., and Wasserman, S.R. (1997) The speciation of uranium in a smectite clay: Evidence for catalysed uranyl reduction. *Radiochimica Acta*, **76,** 113–121.

Grenthe, I., Fuger, J., Konings, R.J.M., Lemire, R.J., Muller, A.B., Nguyen-Trung, C., and Wanner, H. (1992) *Chemical Thermodynamics of Uranium: Nuclear Energy Agency, Chemical Thermodynamics, Volume 1*. North-Holland Elsevier Science, New York, 715 pp.

Hudson, E.A., Rehr, J.J., and Bucher, J.J. (1995) Multiple-scattering calculations of the uranium L_3-edge x-ray-absorption near-edge structure. *Physical Review B*, **52,** 13815–13826.

Hudson, E.A., Allen, P.G., Terminello, L.J., Denecke, M., and Reich, T. (1996) Polarized x-ray absorption spectra of the uranyl ion: Comparison of theory and experiment. *Physical Review B*, **54,** 156–165.

Lemire, R.J. and Tremaine, P.R. (1980) Uranium and plutonium equilibra in aqueous solutions to 200°C. *Journal of Chemical and Engineering Data*, **25,** 361–370.

MacEwan, D.M.C. and Wilson, M.J. (1980) Interlayer and intercalation complexes of clay minerals. In *Crystal Structures of Clay Minerals and Their X-ray Identification*, G.W. Brindley and G. Brown, eds., Mineralogical Society, London, 197–248.

Nguyen, S.N., Silva, R.J., Weed, H.C., and Andrews, J.E., Jr. (1992) Standard Gibbs free energies of formation at the temperature 303.15 K of four uranyl silicates: Soddyite, uranophane, sodium boltwoodite, and sodium weeksite. *Journal of Chemical Thermodynamics*, **24,** 359–376.

Petiau, J., Calas, G., Petitmaire, D., Bianconi, A., Benfatto, M., and Marcelli, A. (1986) Delocalized versus localized unoccupied 5f states and the uranium site structure in uranium oxides and glasses probed by x-ray-absorption near-edge structure. *Physical Review B*, **34,** 7350–7631.

Prikryl, J.D., Pabalan, R.T., Turner, D.R., and Leslie, B.W. (1994) Uranium sorption on α-alumina: Effects of pH and

https://doi.org/10.1346/CCMN.1999.0470406 Published online by Cambridge University Press

surface-area/solution-volume ratio. *Radiochimica Acta*, **66/77,** 291–296.

Rehr, J.J., Mustre de Leon, J., Zabinsky, S.I., and Albers, R.C. (1991) Theoretical X-ray Absorption Fine Structure Standards. *Journal of the American Chemical Society*, **113,** 5135–5140.

Reich, T., Moll, H., Denecke, M.A., Geipel, G., Bernhard, G., Nitsche, H., Allen, P.G., Bucher, J.J., Kaltsoyannis, N., Edelstein, N.M., and Shuh, D.K. (1996) Characterization of hydrous uranyl silicate by EXAFS. *Radiochimica Acta*, **74,** 219–223.

Sawhney, B.L. (1967) Interstratification in vermiculite. *Clays and Clay Minerals*, **15,** 75–84.

Sposito, G. (1984) *The Surface Chemistry of Soils*. Oxford University Press, New York, 234 pp.

Suib, S.L., Tanguay, J.F., and Occelli, M.L. (1986) Comparison of the photochemical and photophysical properties of clays, pillared clays, and zeolites. *Journal of the American Chemical Society*, **108,** 6972–6977.

Taylor, J.C. (1971) The structure of the α form of uranyl hydroxide. *Acta Crystallographica B*, **27,** 1088–1091.

Templeton, D.H. and Templeton, L.K. (1982) X-ray dichroism and polarized anomalous scattering of the uranyl ion. *Acta Crystallographica A*, **38,** 62–67.

Tsunashima, A., Brindley, G.W., and Bastovanov, M. (1981) Adsorption of uranium from solutions by montmorillonite: Compositions and properties of uranyl montmorillonites. *Clays and Clay Minerals*, **29,** 10–16.

Waite, T.D., Davis, J.A., Payne, T.E., Waychunas, G.A., and Xu, N. (1994) Uranium(VI) adsorption to ferrihydrite: Application of a surface complexation model. *Geochimica et Cosmochimica Acta*, **58,** 5465–5478.

(Received 20 March 1998; accepted 10 December 1998; Ms. 98-036)

https://doi.org/10.1346/CCMN.1999.0470406 Published online by Cambridge University Press